Chemical Communications c4cc01984a

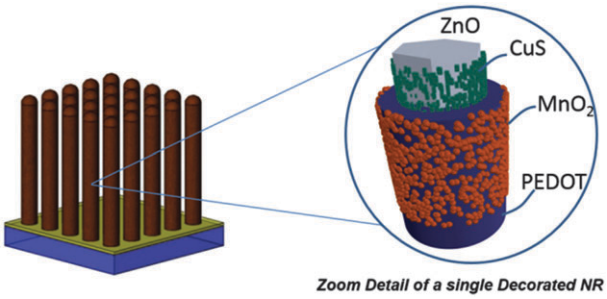

Vertically aligned ZnO@CuS@PEDOT core@shell nanorod arrays decorated with MnO_2 nanoparticles for a high-performance and semi-transparent supercapacitor electrode

Jorge Rodríguez-Moreno,* Elena Navarrete-Astorga, Enrique A. Dalchiele, Ricardo Schrebler, José R. Ramos-Barrado and Francisco Martín

A semi-transparent supercapacitor electrode with hybrid nano-architecture and great specific capacitance that employed covellite to improve the electron transfer is reported.

Please check this proof carefully. **Our staff will not read it in detail after you have returned it.**

Translation errors between word-processor files and typesetting systems can occur so the whole proof needs to be read. Please pay particular attention to: tabulated material; equations; numerical data; figures and graphics; and references. If you have not already indicated the corresponding author(s) please mark their name(s) with an asterisk. Please e-mail a list of corrections or the PDF with electronic notes attached – do not change the text within the PDF file or send a revised manuscript. Corrections at this stage should be minor and not involve extensive changes. All corrections must be sent at the same time.

Please bear in mind that minor layout improvements, e.g. in line breaking, table widths and graphic placement, are routinely applied to the final version.

Please note that, in the typefaces we use, an italic vee looks like this: ν, and a Greek nu looks like this: ν.

We will publish articles on the web as soon as possible after receiving your corrections; **no late corrections will be made.**

Please return your **final** corrections, where possible within **48 hours** of receipt, by e-mail to: chemcomm@rsc.org

Queries for the attention of the authors

Journal: **ChemComm**

Paper: **c4cc01984a**

Title: **Vertically aligned ZnO@CuS@PEDOT core@shell nanorod arrays decorated with MnO_2 nanoparticles for a high-performance and semi-transparent supercapacitor electrode**

Editor's queries are marked on your proof like this Q1, Q2, etc. and for your convenience line numbers are indicated like this 5, 10, 15, ...

Please ensure that all queries are answered when returning your proof corrections so that publication of your article is not delayed.

Query reference	Query	Remarks
Q1	For your information: You can cite this article before you receive notification of the page numbers by using the following format: (authors), Chem. Commun., (year), DOI: 10.1039/c4cc01984a.	
Q2	Please carefully check the spelling of all author names. This is important for the correct indexing and future citation of your article. No late corrections can be made.	
Q3	The GA text has been altered for clarity, please check that the meaning is correct.	
Q4	The sentence beginning "In fact, supercapacitors are devices..." has been altered for clarity, please check that the meaning is correct.	
Q5	The sentence beginning "According to the..." has been altered for clarity, please check that the meaning is correct.	
Q6	The sentence beginning "It can be demonstrated ..." has been altered for clarity, please check that the meaning is correct.	

ChemComm

COMMUNICATION

Vertically aligned ZnO@CuS@PEDOT core@shell nanorod arrays decorated with MnO_2 nanoparticles for a high-performance and semi-transparent supercapacitor electrode†

Cite this: DOI: 10.1039/c4cc01984a

Received 17th March 2014,
Accepted 14th April 2014

DOI: 10.1039/c4cc01984a

www.rsc.org/chemcomm

Jorge Rodríguez-Moreno,*[a] Elena Navarrete-Astorga,[a] Enrique A. Dalchiele,[b] Ricardo Schrebler,[c] José R. Ramos-Barrado[a] and Francisco Martín[a]

Hybrid nano-architectures with high electrochemical performance for supercapacitors have been designed by growing hierarchical ZnO NRs@CuS@PEDOT@MnO_2 core@shell heterostructured nanorod arrays on ITO/glass substrates. This hybrid nano-structured electrode exhibits excellent electrochemical performance, with a high specific areal capacitance of 19.85 mF cm^{-2}, good rate capability, cycling stability and diffused coloured transparency.

Supercapacitors, electrochemical energy storage devices, have attracted growing interest in the last few years. In 2008, a US Department of Energy report assigned equal importance to supercapacitors and batteries for future energy storage systems.[1b] In fact, supercapacitors are devices which are emerging as good feasible alternatives to complement or replace batteries, due to their high power density, high reliability and fast charge–discharge rates.[1a,b] Supercapacitors are power devices that can be fully charged or discharged in seconds, with high power delivery density achieving 10 kW kg^{-1}.[1b] Applications such as memory back-up systems, uninterruptible power supplies, and hybrid electric vehicles coupled with fuel cells or secondary batteries to deliver high power for vehicle acceleration and store the energy converted from braking are in use nowadays.[2–5] However, the major barrier that hinders many practical applications of existing supercapacitors is their low energy density (*ca.* twenty times lower than batteries).[6] So, it is a challenge to find high performance electrode materials (*i.e.*, high specific capacitance as well as good rate capability) with low-cost, environmental benignity and natural abundance.[7] According to the charge–discharge mechanism as well as the active materials used, supercapacitors can be classified as:[1b,8] (i) electrochemical double layer capacitors (EDLCs), involving adsorption–desorption of ions at the electrode/electrolyte interface employing carbon-active (or metallic) materials with high surface area,[8] and (ii) pseudo-capacitors or redox supercapacitors using fast and reversible surface or near-surface reactions for charge storage, mainly by transition metal oxides as well as electrically conducting polymers. On the other hand, transparent energy conversion and storage devices have recently attracted increasing attention due to their great potential to act as integrated power sources for displays, electrochromic devices and smart windows, for instance: glazing systems, automobiles and aerospace vehicles.[9] To the best of our knowledge, no supercapacitor device has been reported to date showing both good transparency and high specific capacitance. In general, claimed percent transmittance values for those electrochemical storage devices reach 60–70% in the visible region, but these devices exhibit very low specific capacitance and capacitance density values, 7.1–64 F g^{-1} and 409 μF cm^{-2}, respectively.[10–12] So, it remains a great challenge to develop supercapacitors with high transparency and high specific capacitance.

In this work, a semi-transparent supercapacitor with a novel architecture and hybrid electrode material with improved capacitive performance was synthesized. This new hybrid electrode material is based on the synergic effects of electrodeposited vertically aligned ZnO NR arrays as nano-structured collectors for support in a core@shell nanostructure of the poly(3,4-ethylenedioxythiophene) (PEDOT) conductive polymer and MnO_2, both being pseudo-capacitive materials. These 1D semiconducting ZnO structures have a high aspect ratio, high surface area, and very high crystalline quality and can provide a direct conduction path for electrons.[13,14] Furthermore, a covellite (CuS) nano-crystalline layer was grown on the ZnO NRs as a good electrical conductor to improve the electron transfer to the nanorod current collector, facilitating the polymer shell to grow on them. This nanostructured electrode will be called the vertically aligned ZnO nanorod arrays@CuS nano-crystalline layer@PEDOT shell layer@MnO_2 nanoparticles hybrid nanocomposite (abbreviated as ZnO NRs@CuS@PEDOT@MnO_2).

[a] *Universidad de Málaga, Andalucía Tech, Departamentos de Física Aplicada & Ingeniería Química, Laboratorio de Materiales y Superficies (Unidad Asociada al CSIC), E29071 Málaga, Spain. E-mail: jromo@uma.es*

[b] *Instituto de Física, Facultad de Ingeniería, Herrera y Reissig 565, C.C. 30, 11000 Montevideo, Uruguay*

[c] *Instituto de Química, Facultad de Ciencias, Pontificia Universidad Católica de Valparaíso, Casilla 4059, Valparaíso, Chile*

† Electronic supplementary information (ESI) available: Experimental procedures including chemical characterization and supplementary figures (Fig. S1–S6). See DOI: 10.1039/c4cc01984a

Its morphological, structural and electrochemical properties were studied. The techniques employed for the synthesis of this hybrid electrode material have the advantages of low growth temperature, low cost and less time consuming compared to those that are based on hard templates (*i.e.* alumina templates).

A schematic illustration of the whole fabrication process of the ZnO NRs@CuS@PEDOT@MnO_2 hybrid electrode is depicted in Scheme 1 (see ESI† for experimental details). Fig. 1 shows the morphological changes of ZnO nanorod arrays before and after the different shell layers growth. Fig. 1a shows typical SEM micrographs of ZnO nanorod arrays electrochemically grown on an ITO/glass substrate. It can be seen that the majority of the nano-pillars are vertically oriented to the substrate plane and the axial direction is aligned with the *c*-axis of the hexagonal ZnO crystal structure. The nanorod mean diameter was 200 nm and the mean length was 1.5 μm giving rise to nanorods with an aspect ratio of about 7.5. Fig. 1b shows a high magnification SEM image of a single ZnO NR, exhibiting an hexagonal cross section and hexagonal faceted and smooth surfaces (which arise due to its wurtzite structure).[15,16] The single crystallinity of the ZnO nanorods is evident from their faceted crystal habit and from XRD results and confirmed by HRTEM analysis as reported in our previously published article.[17] Fig. 1c shows a SEM image of a similar single ZnO NR where, in a second step, the covellite (CuS) nano-crystalline layer was grown by spray-pyrolysis. This CuS nano-crystalline layer has been deposited onto the ZnO NRs not only to enhance charge-transport ability along each single ZnO NR but to provide heterogeneous nucleation sites for the growth of the PEDOT layer. The nanorods in panel 1c do not retain the hexagonal faceted geometry exhibited by the bare ZnO NRs in panel 1b, and the top ends of the nanorods become slightly rounded. Moreover, the SEM image presented in Fig. 1c revealed that the surface of the NR became rough and grainy compared to the very smooth surface without the growth of the CuS nano-crystalline coating (Fig. 1a and b), and the diameters of the nanorod increased. It can be demonstrated that this CuS layer is composed of nano-crystalline aggregates. Afterwards, and in a third step, a PEDOT conductive polymer shell layer was grown on the ZnO NRs@CuS nanorods by electropolymerization of the EDOT monomer. Finally, and in order to grow the MnO_2 nanoparticles, the ZnO NR@CuS@PEDOT samples were soaked in $KMnO_4$ solution. Then, through a redox exchange process, decoration of the ZnO NR@CuS@PEDOT nanostructures by MnO_2 nanoparticles was achieved. Fig. 1d shows a SEM image of a single ZnO NR@CuS@PEDOT@MnO_2 nanostructure which suggests that a PEDOT layer could be successfully deposited onto the surface of the ZnO NRs@CuS nanorods along their entire length, *i.e.* in a conformal way, to eventually form a core–shell structure. Moreover, over the smooth PEDOT layer, the presence of the MnO_2 NPs can be inferred from the roughness that the ZnO NR@CuS@PEDOT@MnO_2 nanostructure exhibits (see Fig. 1d). It must be pointed out that even with three components integrated, the uniform array structure is still retained. So, nearly all the hybrid core–shell NRs are highly accessible to electrolytes for electrochemical energy storage due to the presence of convenient diffusion channels. The detailed microstructure and the chemical composition of the ZnO NR@CuS@PEDOT@MnO_2 nanostructure are further investigated by transmission electron microscopy (TEM)-related techniques. The spatial distribution of the compositional elements (Zn, O, S, Mn and Cu) within the ZnO NR@CuS@PEDOT@MnO_2 nanorods was obtained using TEM-EDX line-scans along the radial direction of the nanorods (marked by a straight line in Fig. 1, image (e)). In the intensity profile of the compositional elements shown in image (e) of Fig. 1, Zn and O signals are mainly confined within the nanorod core area, while a higher intensity of Cu, S and Mn is found in the shell region. This is consistent with the ZnO NR@CuS@PEDOT@MnO_2 core–shell nanorod configuration observed in the TEM images (*vide infra*). Fig. 1f shows a TEM image of a single ZnO

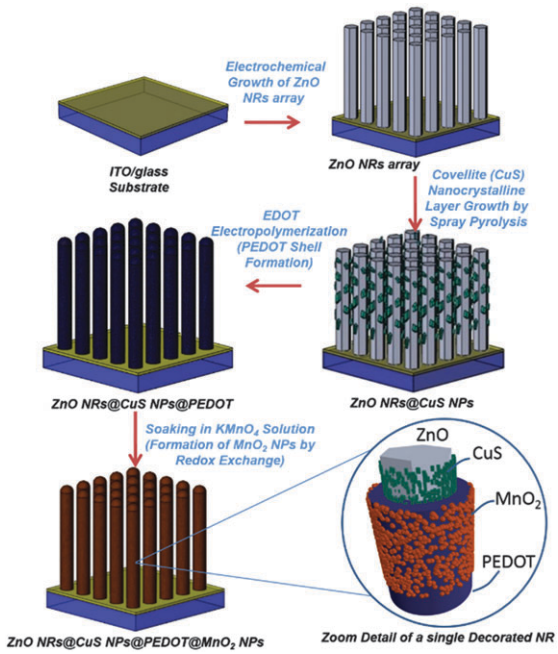

Scheme 1 Schematic illustration of the synthesis process for the designed ZnO NRs@CuS@PEDOT@MnO_2 hybrid nanostructured electrode.

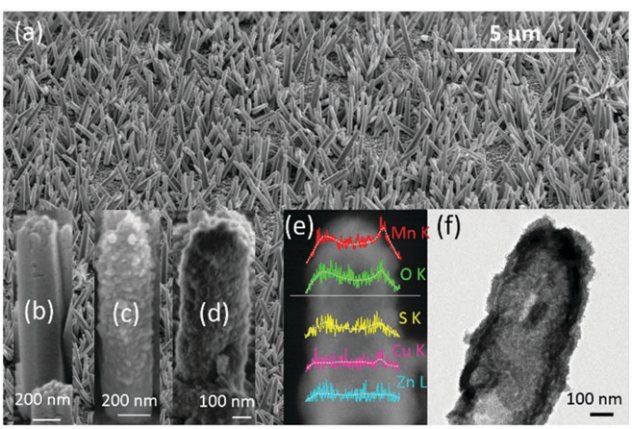

Fig. 1 (a) 52° titled SEM image of bare ZnO nanorod arrays on the ITO/glass substrate. (b) Bare single ZnO NR, (c) single ZnO nanorod densely coated CuS nano-crystal shell. (d) Single nanorod, (e) EDX line-scan and (f) TEM image of ZnO NR@CuS@PEDOT@MnO_2.

NR@CuS@PEDOT@MnO_2 nanorod detached from the ITO/glass substrate. From this TEM picture it can be found that the PEDOT layer covers the ZnO@CuS nanorod. The average thickness of the polymer wall is approximately 50 nm. Dimly observable, dark dots of approximately 5 nm assigned to MnO_2 nanoparticles are found in the outer part of the nanorod image. Raman, ATR-FTIR and XPS of the ZnO NRs@CuS@PEDOT@MnO_2 synthesized nano-pillar arrays are shown in Fig. S1, S3, S5 in the ESI.† XPS analysis confirms the 4+ oxidation state of manganese with $2p_{3/2}$ and $2p_{1/2}$ peaks located at 642 and 653.6 eV and a new peak at 168 eV in the S 2p region indicates sulphur-oxidation of the PEDOT thiophene ring to the sulfone group (R–SO_2–R) by $KMnO_4$ (Fig. S2 and S5†).

The electrochemical performance of the nanostructured ZnO NRs@CuS@PEDOT@MnO_2 electrode was examined by standard cyclic voltammetry (CV), the galvanostatic charge–discharge technique and electrochemical impedance spectroscopy (EIS). Fig. 2a shows the CV curves at different scan rates of a ZnO NRs@CuS@PEDOT@MnO_2 electrode in 1 M $LiClO_4$ aqueous electrolyte. It is shown that all the CV curves are almost quasi-rectangular with symmetric shape at these scanning rates, suggesting that hybrid nanostructured electrodes with fast reversible reaction and an ideal capacitive behaviour were obtained. The electrode maintains this nearly rectangular waveform (even at 100 mV s^{-1}), indicating fast pseudocapacitive behaviour and proving that the overall polymer surrounded nanorod structure enables fast access of ions to the surface of MnO_2. Distorted shape is associated with higher electronic resistance of the electrode sheet and mass transport resistance in the electrolyte.[18] Only weak redox peaks at −0.2 V and 0.2 V *vs.* SME can be found in Fig. 2a in agreement with that reported by other authors,[19–21] due to pseudocapacitance overlapping from conducting polymer interaction. In fact, different electrochemical behaviors can be observed from the CV shape providing the ion diluted in the electrolyte. The K-ion, for instance, displays two well-defined peaks, whereas the Li-ion and the Na-ion exhibit minor peaks combined with a quasi-rectangular shape.[21] Capacitance of manganese oxides comes mainly from pseudocapacitance, ascribed to reversible redox reactions in conjunction with the intercalation/adsorption of protons and/or cations. In aqueous electrolytes, the charge storage mechanism of MnO_2 could be described by the following electrochemical reactions between MnO_2 and the electrolyte, with (i) possible bulk intercalation or deintercalation of Li^+ or H_3O^+:[22]

$$(MnO_2)_{bulk} + M^+ + e^- \leftrightarrow (MnOOM)_{bulk},\ M^+ = Li^+ \text{ or } H_3O^+ \quad (1)$$

and/or (ii) adsorption of the cation on the surface:[23]

$$(MnO_2)_{surface} + M^+ + e^- \leftrightarrow (MnO_2{}^-M^+)_{surface},\ M^+ = Li^+ \text{ or } H_3O^+ \quad (2)$$

Fig. 2b shows the galvanostatic charge–discharge curves of the ZnO NRs@CuS@PEDOT@MnO_2 hybrid nanostructured electrode at current densities of 50, 100, 150 and 200 μA cm^{-2}. The charge–discharge curves display a symmetric and nearly linear shape, indicating that the hybrid nanostructured electrode has outstanding super-capacitive behaviour.

From the CV curves and from the charge–discharge measurements conducted on the ZnO NRs@CuS@PEDOT@MnO_2 hybrid nanostructured electrode (Fig. 2a and b, respectively), its specific areal capacitances C_{area} at different scan rates and current densities were calculated. As pointed out by Gogotsi and Simon,[23] the weight of the active film is negligible compared to the stack device and it is not possible to scale it up linearly, therefore the areal capacitance is much more a reliable performance metric for supercapacitor devices compared to gravimetric capacitance. Thus, all of the capacitance values of the supercapacitor electrodes are evaluated in area units, if not otherwise specified. The calculated specific areal capacitance from CV curves is 19.85 mF cm^{-2} at the scan rate of 5 mV s^{-1}, retaining most of its capacitance (14.20 mF cm^{-2}) even at 100 mV s^{-1}. The decrease of the specific capacitance with increasing scan rate can be ascribed to the reduced time for insertion/extraction of protons or alkali cations into MnO_2 at a high scan rate.[24] The specific areal capacitance values obtained from the charge–discharge curves were calculated to be 12.47 mF cm^{-2} at a current density of 50 μA cm^{-2} and 11.01 mF cm^{-2} at 200 μA cm^{-2}.

These specific areal capacitance values as a function of current density suggest excellent rate capability, with 88% capacitance remaining when the current density is increased 4 fold. As reported in literature, the decrease in specific capacitance with increasing current density can be due to the internal resistance of electrodes.[22,25] It can be seen that the specific capacitance values obtained from the charge–discharge curves are almost comparable with those obtained from CV curves. These results are much better than the reported C_{area} value for other nanostructured electrode systems such as highly ordered MnO_2 nanopillars (6.13 mF cm^{-2}),[6] interdigital graphene oxide–carbon nanotube composites (5.1 mF cm^{-2}) and single walled carbon nanotubes (3.47 mF cm^{-2}).[26,27] On the other hand, the C_{area} values reported here are comparable to that of a MnO_2/H-TiO_2 on a Ti fiber supercapacitor electrode (18.3 mF cm^{-2}).[28] Such superior performance of the

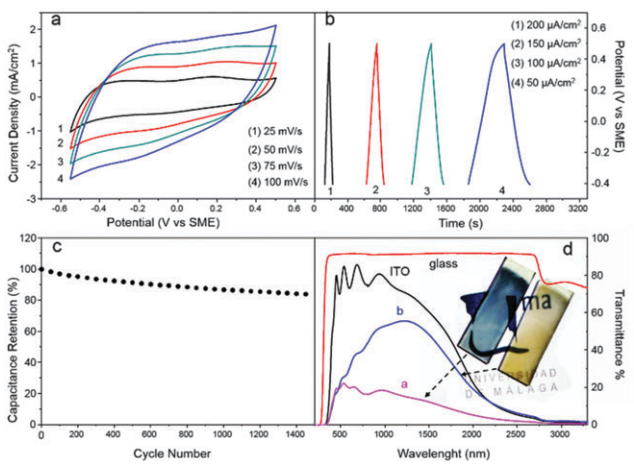

Fig. 2 (a) CV curves, (b) galvanostatic charge–discharge and (c) capacitance retention *vs.* cycle numbers of the ZnO NRs@CuS@PEDOT@MnO_2 nanostructured electrode. (d) Transmittance spectra of glass, ITO/glass, the studied electrode without (spectrum a) and with MnO_2 (spectrum b) and digital photography of both samples.

hierarchical ZnO NRs@CuS@PEDOT@MnO_2 hybrid nanostructured electrode must be related to its unique structure and large specific surface area. In more detail, this might be attributed to different possible key factors. First, the large contact area between the current collector and active material can significantly shorten the electron transportation path length.[6] Second, decorating active nanomaterial on nanostructured current collectors leads to the increase in the number of electrochemically active sites for the redox reaction. This facilitates rapid diffusion of the cations during the charging–discharging process.[6] Third, densely arranged ZnO NRs@CuS@PEDOT nanopillars on the ITO/glass substrate offer more electrochemically active sites for nucleation and growth of MnO_2.[6] Fourth, the existence of the CuS@PEDOT shell layer can provide more effective charge-transport routes along each single ZnO nanorod.[8]

The long-term cycling stability is one of the most critical factors and is a valuable test to evaluate supercapacitor applications. Fig. 2c shows the resulting specific capacitance retention of a ZnO NRs@CuS@PEDOT@MnO_2 hybrid nanostructured electrode as a function of CV cycle numbers. These data were collected by repeating the CV test between −0.4 V and 0.5 V at a scan rate of 100 mV s^{-1}. The specific capacitance retention of the hybrid nanostructured electrode is quite stable and loses only 18% of the initial capacitance after 1500 cycles, indicating great cycling stability. Furthermore, it clearly shows that the performance is not limited by parasitic chemical reactions and mechanical breakdown due to swelling of the electrode or mechanical strain during the charging–discharging process.[29]

Fig. 2d shows the optical transmittance *vs.* wavelength spectra of glass, the ITO-glass substrate, and the studied electrode without and with MnO_2 (curves a and b, respectively). The samples without and with MnO_2 exhibit at 700 nm transmittance values of 20% and 40%, respectively, close to 55% reported by Tao Chen *et al.*,[10] but with three orders of magnitude greater specific areal capacitance; and with similar transmittance values reported by Chen *et al.*[12] in the visible region of *ca.* 30%–60%. Photograph images of the electrodes (inset of Fig. 2d) exhibit colored transparency promptly applicable in glazing systems, skylight structures or vanguard technological innovations. Diffusive light created by this sample is suitable for the indoor architectural environment. Interestingly, $KMnO_4$ oxidation reaction of PEDOT improves the transparency of the polymer from pale blue in the reduced state to an almost colorless bleached oxidized state,[30] preventing increased opacity with the MnO_2 shell decoration.

In conclusion, a facile, low cost, less time consuming and scalable strategy has been developed to construct semi-transparent hierarchical ZnO NRs@CuS@PEDOT@MnO_2 hybrid nano-architectures with high electrochemical performance for supercapacitors. This hybrid nano-structured electrode exhibits excellent electrochemical performance, with a high specific areal capacitance of 19.85 mF cm^{-2}, good rate capability and cycling stability. Such stimulating capacitive behavior is attributed to the unique hierarchical core–shell hybrid nanorod array configuration and the synergistic effects of ZnO NR current collectors and the combined pseudocapacitive contributions from the PEDOT@NPs MnO_2 shell layer. Moreover, the ZnO NRs@CuS@PEDOT@MnO_2 electrode showed diffused colored transparency suitable for vanguard technological innovations.

The authors are grateful to MINECO of Spain, for the financial support received (Consolider Ingenio 2010 FUNCOAT-CSD2008-00023). This work was partially supported by CSIC (Comisión Sectorial de Investigación Científica) of the Universidad de la República, in Montevideo, Uruguay, and PEDECIBA—Física. The authors are grateful for the support received from the D.I.-Pontificia Universidad Católica de Valparaíso, Valparaíso, Chile.

Notes and references

1 (*a*) J. R. Miller and P. Simon, *Science*, 2008, **321**, 651; (*b*) P. Simon and Y. Gogotsi, *Nat. Mater.*, 2008, **7**, 845.
2 J. Moreno, M. E. Ortúzar and J. W. Dixon, *IEEE Trans. Ind. Electron.*, 2006, **53**, 614.
3 L. U. Gökdere, K. Benlyazid, R. A. Dougal, E. Santi and C. W. Brice, *Mechatronics*, 2002, **12**, 575.
4 P. Thounthong, S. Räel and B. Davat, *J. Power Sources*, 2006, **158**, 806.
5 L. T. Lam and R. Louey, *J. Power Sources*, 2006, **158**, 1140.
6 Z. Yu, B. Duong, D. Abbitt and J. Thomas, *Adv. Mater.*, 2013, **24**, 3302.
7 M. Yu, H. Sun, X. Sun, F. Lu, G. Wang, T. Hu, H. Qiu and J. Lian, *Int. J. Electrochem. Sci.*, 2013, **8**, 2313.
8 Y. Zhao and P. Jiang, *Colloids Surf., A*, 2014, **444**, 232.
9 Z. Xie, X. Jin, G. Chen, J. Xu, D. Chen and G. Shen, *Chem. Commun.*, 2014, **50**, 608.
10 T. Chen, Y. Xue, A. K. Roy and L. Dai, *ACS Nano*, 2014, **8**, 1039.
11 H. Y. Jung, M. B. Karimi, M. G. Hahm, P. M. Ajayan and Y. J. Jung, *Sci. Rep.*, 2012, **2**, 773.
12 P.-C. Chen, G. Shen, S. Sukcharoenchoke and C. Zhou, *Appl. Phys. Lett.*, 2009, **94**, 043113.
13 V. Consonni, G. Rey, J. Bonaimé, N. Karst, B. Doisneau, H. Roussel, S. Renet and D. Bellet, *Appl. Phys. Lett.*, 2011, **98**, 111906.
14 J. Chung, J. Myoung, J. Oh and S. Lim, *J. Phys. Chem. C*, 2010, **114**, 21360.
15 C. D. Bojorge, V. R. Kent, E. Teliz, H. R. Cánepa, R. Henríquez, H. Gómez, R. E. Marotti and E. A. Dalchiele, *Phys. Status Solidi A*, 2011, **208**, 1662.
16 T. Pauporté, Z. M. Wang, A. Waag, G. Salamo, N. Kishimoto, S. Bellucci and Y. J. Park, *Toward Functional Nanomaterials*, Springer Science+Business Media, LLC, 2009.
17 J. Rodríguez-Moreno, E. Navarrete-Astorga, R. Romero, F. Martín, R. Schrebler, J. R. Ramos-Barrado and E. A. Dalchiele, *Thin Solid Films*, 2013, **548**, 235.
18 R. Liang, H. Cao and D. Qian, *Chem. Commun.*, 2011, **47**, 10305.
19 Z. Su, C. Yang, C. Xu, H. Wu, Z. Zhang, T. Liu, C. Zhang, Q. Yang, B. Lia and F. Kang, *J. Mater. Chem. A*, 2013, **1**, 12432.
20 L. Su, L. Gong, H. Lü and Q. Xü, *J. Power Sources*, 2014, **248**, 212.
21 P. Sen, A. Deb, A. D. Chowdhury, S. K. Bandyopadhyay, N. Agnihotri and M. Mukherjee, *Electrochim. Acta*, 2013, **108**, 265.
22 X. Sun, Q. Li, Y. Lu and Y. Mao, *Chem. Commun.*, 2013, **49**, 4456.
23 Y. Gogotsi and P. Simon, *Science*, 2011, **334**, 917.
24 S. Li, J. Wen, X. Mo, H. Long, H. Wang, J. Wang and G. Fang, *J. Power Sources*, 2014, **256**, 206.
25 R. B. Rakhi, W. Chen, D. Cha and H. N. Alshareef, *Nano Lett.*, 2012, **12**, 2559.
26 M. Beidaghi and C. Wang, *Adv. Funct. Mater.*, 2012, **22**, 4501.
27 X. Li, T. Gu and B. Wei, *Nano Lett.*, 2012, **12**, 6366.
28 X. Lu, G. Wang, T. Zhai, M. Yu, J. Gan, Y. Tong and Y. Li, *Nano Lett.*, 2012, **12**, 1690.
29 R. B. Ambade, S. B. Ambade, N. K. Shrestha, Y.-C. Nah, S.-H. Han, W. Lee and S.-H. Lee, *Chem. Commun.*, 2013, **49**, 2308.
30 J. P. Lock, J. L. Lutkenhaus, N. S. Zacharia, S. Gap Im, P. T. Hammond and K. K. Gleason, *Synth. Met.*, 2007, **157**, 894.

